ACI STRUCTURAL JOURNAL TECHNICAL PAPER

Title no. 103-S26

Compression Field Modeling of Fiber-Reinforced Concrete Members Under Shear Loading

by Fausto Minelli and Frank J. Vecchio

Several laboratory experiments have demonstrated the effectiveness of steel fibers in substituting the minimum code-required shear reinforcement in beams, particularly in precast high-performance concrete structures. Despite the large number of experimental results available, only a few numerical studies have been published concerning fiber-reinforced concrete structures. The behavior of different kinds of full-scale steel fiber-reinforced concrete elements is analyzed herein using a finite element code based on the modified compression field theory (MCFT) and the disturbed stress field model (DSFM), and suitably adapted for steel fiber reinforcement. The numerical model is validated against the experimental results obtained on full-scale fiber-reinforced concrete (FRC) structural elements and is shown to adequately simulate the strength, stiffness, ductility, crack pattern development, and failure modes of all specimens tested, including those lightly reinforced or with fibers only.

Keywords: cracking; fiber-reinforced concrete; shear; tension.

INTRODUCTION

The behavior and design of reinforced concrete beams in shear remains an area of concern. Design codes are continually changing and generally becoming more stringent. There remains a pressing need to establish design and analysis methods that provide realistic assessments of the strength, stiffness, and ductility of structural elements under shear loading.

The use of fiber-reinforced, high-performance concrete (FRHPC) has gained considerable attention in recent years, particularly when crack propagation control is of primary importance, such as in slab-on-ground applications[1] or in beams where shear reinforcement is partly or totally absent.[2-5] The use of FRHPC in the precast industry may become particularly appealing if it can be demonstrated that sufficient strength and ductility can be reached in prestressed beams even in the absence of shear reinforcement.[6] From a practical point of view, however, current design codes do not usually include any statement on fiber-reinforced concrete (FRC) that could allow engineers to incorporate fibrous reinforcement in their structural designs. This occurs despite extensive research on its material properties that has now made FRC well known.

Numerical modeling of the nonlinear behavior of FRHPC materials requires the use of advanced computer codes, which implement material nonlinearities and allow the correct modeling of concrete fracture phenomena, fundamental when crack development and propagation significantly influence the structural response.

The modified compression field theory (MCFT) is a well-known model for representing the nonlinear behavior of reinforced concrete structures. It is essentially a smeared, rotating crack model for cracked reinforced concrete elements.[7] On the basis of a number of panel tests, constitutive relationships were developed describing the behavior of cracked reinforced concrete in compression and in tension. Those models were incorporated into new design procedures[8] (for example, those that form the basis for the general method for shear design in the Canadian Code, CSA A23.3-04), and into the formulation of various nonlinear finite elements algorithms. The resulting analysis procedures have been shown to provide accurate simulations of response for a wide range of structures including beams in flexure, shear and torsion, deep beams, shearwalls, columns, and plate and shells.

In lightly reinforced elements, however, where crack shear slip is significant, the rotation of the principal stress field tends to lag the greater rotation of the principal strain field. For such elements, the shear stiffness and strength is generally slightly overestimated by the MCFT, which assumes the rotations are equal. The disturbed stress field model (DSFM)[9-11] was developed to address this and other systematic deficiencies of the MCFT in predicting the response of certain structures and loading scenarios. The DSFM is conceptually similar to the MCFT but extends the MCFT in several respects. Most importantly, the DSFM augments the compatibility relationships of the MCFT to include crack shear slip deformations. The strains due to these deformations are distinguished from the strains of the concrete continuum due to stress. As such, the DSFM decouples the orientation of the principal stress field from that of the principal strain field, resulting in a smeared delayed rotating-crack model. Moreover, by explicitly calculating crack slip deformations, the DSFM eliminates the crack shear check as required by the MCFT. Constitutive relationships for concrete and reinforcement are also refined.

In the present paper, the results of nonlinear analyses performed on three different sets of prestressed FRHPC beams (having different geometry, reinforcement, and fiber amount) subjected to shear, tested at the University of Brescia, Italy, are presented. The main purpose of that experimental program was to investigate the possibility of partially or totally replacing the transverse reinforcement (stirrups) with fibers, and to analyze the failure mechanisms with and without fibers. In doing so, four prestressed I-shaped beams, three prestressed open section thin-webbed roof elements, and three shear-critical beams were tested. All specimens were made of high-strength concrete (HSC). The experimental results were found to be highly useful in proving the effectiveness of fibers,

ACI Structural Journal, V. 103, No. 2, March-April 2006.
MS No. 04-290 received September 9, 2004, and reviewed under Institute publication policies. Pertinent discussion including author's closure, if any, will be published in the January-February 2007 *ACI Structural Journal* if the discussion is received by September 1, 2006.

ACI member **Fausto Minelli** *is participating in a postdoctoral fellowship in the Department of Civil Engineering, the University of Brescia, Brescia, Italy. He received his BSc and PhD in structural engineering from the University of Brescia in 2001 and 2005, respectively. His research interests include shear behavior of lightly transverse reinforced beams, high-performance concrete, fiber-reinforced concrete, and nonlinear analyses of reinforced concrete structures.*

Frank J. Vecchio, *FACI, is a professor of civil engineering at the University of Toronto, Toronto, Ontario, Canada. He is a member of Joint ACI-ASCE Committees 441, Reinforced Concrete Columns, and 447, Finite Element Analysis of Reinforced Concrete Structures. His research interests include constitutive modeling of reinforced concrete, development of nonlinear analysis, and repair and rehabilitation of concrete structures.*

which in all three types of structures resulted in an increase in ductility and strength; the enhanced ductility, in turn, led to a flexural failure rather than a shear collapse, as exemplified in two identical beams, one cast with the reference (plain) concrete while the other with high strength fibers.[12]

The numerical analyses of the beams were carried out adopting a two-dimensional plane stress finite element (FE) model based on the MCFT and DSFM. In modeling the different structures, particular attention was devoted to the nonlinear behavior of the materials, especially with regard to FRC. Moreover, the program was modified by adding new tension softening relationships for the fibrous reinforcements used and, without stirrups, carefully considering the crack width limits.

A major objective of the analyses undertaken was to study the development of shear resistant mechanisms in beams with and without shear reinforcement in detail. An accurate evaluation of the fiber contribution to shear resistance was also sought. The analyses would also provide a measure of the accuracy and the reliability of the MCFT and DSFM in predicting the actual behavior of SFRC structural elements. Details and results of these studies are presented herein.

RESEARCH SIGNIFICANCE

This paper addresses the applicability and accuracy of MCFT-based procedures to the analyses of a wide range of structural elements mainly cast with randomly distributed fibers as an additional (or the only) shear reinforcement provided. It shows that a smeared delayed rotating-crack analyses gives an accurate representation of fiber-reinforced beams under shear, provided that particular attention is devoted to the tension softening behavior and the crack limits assumed. Some considerations regarding these two latter parameters, which are critical for an adequate representation of the real behavior, are also be presented and discussed.

DETAILS OF TEST SPECIMENS

A set of numerical analyses was performed on:

- Four high-performance concrete beams having the geometry shown in Fig. 1(a) (Specimens I-Beam1, I-Beam2, I-Beam3, and I-Beam4);
- Three thin-webbed open section roof elements having the geometry depicted in Fig. 1(b). (Specimens R-ElemWM, R-Elem45, and R-Elem80); and
- Three high strength concrete shear-critical beams having the geometry shown in Fig. 1(c). (Specimens SC-BeamPC, SC-Beam45, and SC-Beam80).

With regard to the first set of experiments,[3] two shear tests were carried out on each beam, adopting the layout illustrated in Fig. 2. The first test concerned Zone TZ (transfer zone), while the second was devoted to Zone DZ (diffused prestressing action zone). Tests in Zone TZ were representative of the beam behavior near the supports, where transverse reinforcement is necessary to improve both the bond

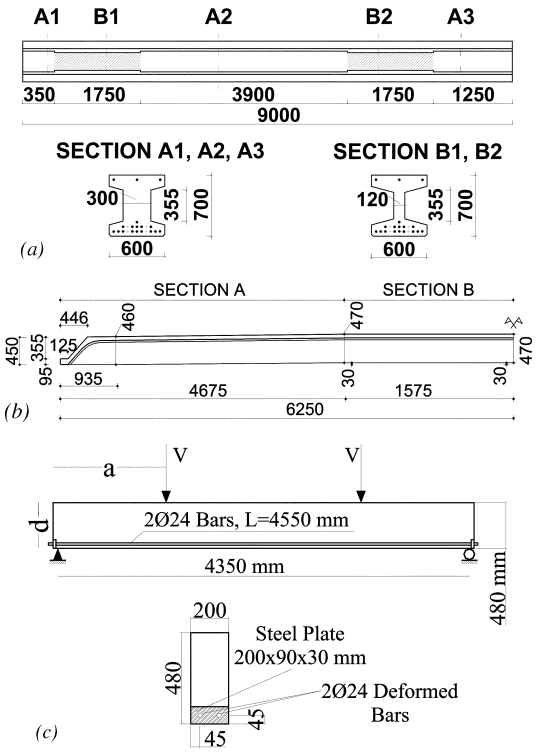

Fig. 1—Geometry of: (a) I-Beam specimens; (b) R-Elem specimens; and (c) SC-Beam specimens.

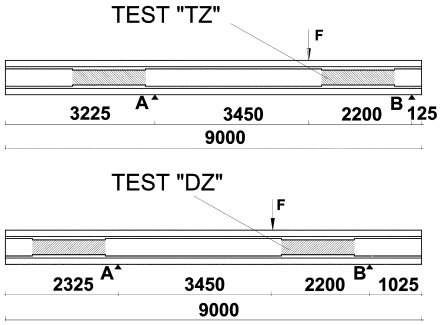

Fig. 2—Loading schemes for two tests on I-Beam specimens.

behavior of the prestressing strands and the shear strength of the beam. Those in Zone DZ represented the behavior in an internal part of the beam, where a minimum reinforcement amount is usually required and the prestressing action is completely diffused.

Two beams (I-Beam1 and I-Beam2) were cast with plain concrete, while 50 kg/m^3 of steel fibers (volume ratio V_f = 0.64%) were added to the remaining beams. Two types of fibers were used: a normal strength fiber (45/30) having a length of 30 mm and an aspect ratio (length/diameter) equal to 45, and a high strength fiber (80/30) having a length of 30 mm and an aspect ratio of 80. Fibers 45/30 were used in I-Beam3 while fibers 80/30 were used in I-Beam4.

All beams were designed according to Eurocode 2 (EC2)[13] provisions to have a shear failure in either of the two test zones. For this reason, the flanges and web outside the experimental zones (the collapse location) were stiffened; the section of the beam along the zones chosen for the shear collapse therefore had the typical geometry of a precast beam with a panel-web thickness equal to 120 mm (refer to Fig. 1(a) and 2).

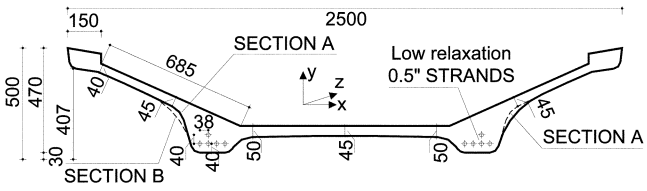

Fig. 3—Geometry of cross section of R-Elem specimens.

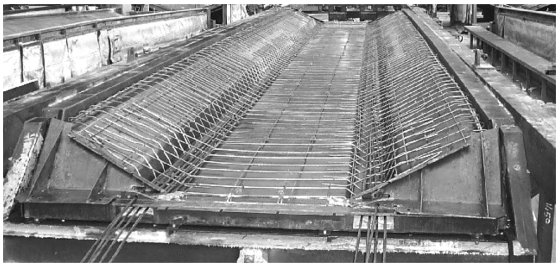

Fig. 4—Transverse reinforcement in R-ElemWM specimens.

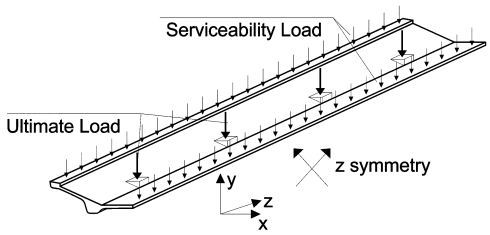

Fig. 5—Loading scheme for R-Elem specimens.

The panel test area was 1.75 m long (five times the web depth), whereas the overall beam length was 9 m (Fig. 2). The beams were simply supported with a span of 5.65 m, and a point load was applied 2.2 m away from support (Fig. 2) to have a constant shear force along the collapse zone (neglecting dead load).

In Zones TZ and DZ, different transverse reinforcement amounts were adopted:

- I-Beam1 was constructed without any transverse reinforcement (neither in the TZ nor in the DZ zones);
- I-Beam2 was cast with transverse reinforcement designed according to EC2.[13] In Zone TZ, the stirrups (ϕ6 at 100 mm) were designed on the basis of a truss mechanism while in Zone DZ, transverse reinforcement was the minimum required by the code (mesh fabric ϕ5 at 200 x 200 mm);
- Zones TZ of I-Beam3 and I-Beam4 were reinforced with the same transverse reinforcement of Beam 2. In these beams, Zones DZ were cast without traditional reinforcing bars, so that steel fibers were the only reinforcement present in the web; and
- In the remaining parts of the beams, ϕ10 at 100 mm stirrups were used.

Regarding the second set of experiments (roof elements), the main purpose of the experimental program was to study the behavior of thin webbed open section elements without traditional transverse reinforcement (which resist shear, torsion, and transverse flexure) and to evaluate the possibility of substituting it with steel fibers.

The specimens were 12,500 mm long (Fig. 1(b)). The cross section, shown in Fig. 3, consisted of a 50 mm thick horizontal slab near the two bottom chords reducing to 45 mm thickness near the middle, and of two variable thickness wings inclined at 35 degrees to the horizontal. The cross section was also slightly thickened in the middle portion of the elements (Fig. 1(b) and 3), leading to a larger lever arm and hence to a greater flexural capacity. The overall cross section was 2500 mm wide while the average height was approximately 450 mm. The open section and 30 mm slope provided (Fig. 1(b)) were intended to facilitate rain drainage. In such situations, the thin webs make flexural-torsion and transverse bending essential checks, even if longitudinal bending remains the critical parameter for the designer. The two symmetric bottom chords were characterized by wide sections to increase the fire protection of the longitudinal steel reinforcement located within.

Different transverse reinforcement was adopted in the three elements tested:

- The first element (R-ElemWM) was constructed with a steel welded-mesh fabric (ϕ5 reinforcing bar every 250 mm in *x*-direction and 200 mm in *y*-direction (refer to Fig. 3); 1ϕ5 at 250 x 200 mm);
- The second roof element (R-Elem45) was reinforced with 50 kg/m^3 (V_f = 0.64%) of low carbon 45/30 fibers; and
- The third element (R-Elem80) was cast with 50 kg/m^3 (V_f = 0.64%) of high carbon 80/30 fibers.

Note that fibers were the only transverse reinforcement in specimens R-Elem45 and R-Elem80. In all cases, however, the specimens were traditionally reinforced for a length of 80 diameters of tendons, corresponding to approximately 1 m (see the greater steel amount at transfer for R-ElemWM in Fig. 4) to enable diffusion of prestressing stresses along the transfer length, shear resistance in the transverse direction, and bulkhead action.

The specimens were loaded by implementing two different test sequences (Fig. 5). In the first, a serviceability live load was applied (corresponding to the snow load required by code) by means of three steel bundles longitudinally distributed along the symmetric axis and the top chords of the element. In the second phase, the ultimate load was applied by using a steel frame displacement-controlled system with eight loading points in order to accurately reproduce a uniformly distributed load. (Fig. 5).

With respect to the last group of elements, three shear-critical beams were tested in order to study the shear contribution due to the fibers themselves, avoiding several variations in other factors (stirrups, geometry, transverse effects, prestressing) that would have made the fiber characterization more complicated.

These beams were 4350 mm long, 480 mm deep, and 200 mm wide (having a rectangular cross section) and were constructed with high strength concrete. They were simply reinforced in the bottom face by 2ϕ24 deformed bars, as shown in Fig. 1(c). All three beams were loaded by means of a steel displacement-controlled frame with a four-point bending scheme (4PBT), choosing the critical shear length so that a/d = 2.5 (refer to Fig. 1(c)). No traditional shear reinforcement was provided in all cases. Specimen SC-BeamPC was made of plain concrete while SC-Beam45 and SC-Beam80 were constructed by adding 50 kg/m^3 (V_f = 0.64%) of 45/30 and 80/30 fibers, respectively, to the matrix. Again, the fibers were the only shear reinforcement provided in the two latter elements described. Moreover, suitable steel plates were designed at both ends of the specimens in order to provide sufficient anchorage to the bars.

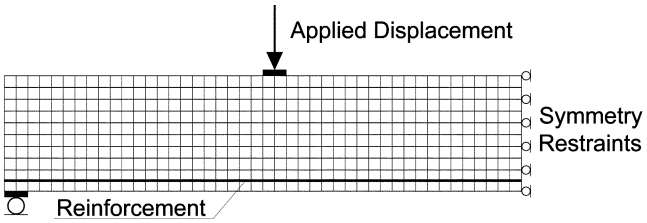

Fig. 6—FE representation of SC-Beam specimens.

Table 1 summarizes the transverse reinforcement details for all specimens considered.

NUMERICAL MODELING OF TEST SPECIMENS

A two-dimensional plane stress model was developed for all three types of test specimens. For the three shear-critical beams (SC-Beam specimens) this was an accurate assumption. In the case of I-Beam specimens, a two-dimensional representation was sufficient enough for adequately simulating the stress distribution, the crack formation, and its development, even at the abrupt section change (B1 and B2 section of Fig. 1(a)) where a three-dimensional model could have been more representative of the actual behavior.

Conversely, a two-dimensional model was not a totally correct assumption for the three open section elements (R-Elem specimens), as transverse flexure turned out to play an important role, especially at the point of structural collapse. Owing to some difficulties in running a proper nonlinear three-dimensional model, however, a two-dimensional model was used. Nevertheless, the experimental results demonstrated few transverse flexure effects for R-Elem45 and R-Elem80 (owing to the bridging effect offered by fibers), while non-negligible transverse flexure effects were observed for R-ElemWM (reinforced with welded fabric mesh), even though overall displacements were quite high. Moreover, ultimate collapse always occurred as a combination of longitudinal and transverse flexure. For these reasons, the two-dimensional model was assumed to be sufficiently reliable and quite accurate, at least for a wide range of displacement of the structure. Figure 6 depicts the mesh constructed for the shear-critical model.

Table 2 summarizes the main features of the meshes adopted for the three different sets of structural elements considered. Note that four-noded elements with uniform thickness were used in all concrete FE representations, while two-noded truss bars with uniform cross-sectional area were adopted for any reinforcement not embedded.

With regard to the reinforcement, different modeling approaches were adopted. Prestressing steel reinforcement (which was present both in the I-Beams and in the roof elements R-Elem, 0.6 and 0.5 low-relaxation strands, respectively) was modeled by using truss elements, linking nodes having the same coordinates and numbers of concrete nodes. Perfect steel-to-concrete bond was therefore assumed. The pretension loading was simulated by applying a prestrain to the cable. The prestrain was chosen equal to the experimental value (taking into account friction and inelastic losses in the amount of 15% of the total initial value). In the transfer zone, a linear development of prestrain was assumed, in order to simulate the transfer phenomenon of the pretensioning from the beam end (no prestrain) to a distance equal to 50 strand diameter (750 to 650 mm, respectively), beyond that, the pretension action was assumed to be uniform and completely developed.

For the I-Beam model, deformed bars (which were placed in order to control crack formation and development, and to allow the structure to achieve greater ductility), stirrups and welded wire mesh were modelled as embedded reinforcement in the concrete elements. Perfect steel-to-concrete bond was also assumed in this case. Conversely, in the SC-Beam model, deformed bars, which were the only flexure reinforcement, were modeled with truss elements, assuming perfect steel-to-concrete bond as well.

Table 1—Summary of experimental program

Specimen	Test	Transverse reinforcement	Concrete $f_{c,cube}$, MPa	Concrete f'_c, MPa	Concrete f_{ct}, MPa	Concrete E_c, MPa	Transverse reinforcement f_{sy}, MPa	Transverse reinforcement f_{st}, MPa
I-Beam1	TZ	No shear reinforcement	84.9	70.5	4.43	41,400	—	—
	DZ	No shear reinforcement	84.9	70.5	4.43	41,400	—	—
I-Beam2	TZ	Stirrups (design reinforcement)	86.1	71.5	3.69	41,600	481	614
	DZ	Mesh (minimum reinforcement)	86.1	71.5	3.69	41,600	575	658
I-Beam3	TZ	Stirrups + 45/30 fibers	82.3	68.3	4.65	44,200	481	614
	DZ	45/30 fibers	82.3	68.3	4.65	44,200	—	—
I-Beam4	TZ	Stirrups + 80/30 fibers	92.8	77.0	5.18	43,100	481	614
	DZ	80/30 fibers	92.8	77.0	5.18	43,100	—	—
R-ElemWM		Welded mesh fabric	72.1	59.8	3.87	38,100	575	658
R-Elem45		45/30 fibers	74.1	61.5	4.10	38,700	—	—
R-Elem80		80/30 fibers	67.0	55.6	3.71	36,500	—	—
SC-BeamPC		No shear reinforcement	72.9	60.5	3.15	34,400	—	—
SC-Beam45		45/30 fibers	73.6	61.1	3.48	36,800	—	—
SC-Beam80		80/30 fibers	70.3	58.3	3.20	32,700	—	—

Table 2—Summary of numerical models

Specimen	Test	Concrete elements	Reinforcement elements	Loading stages	MCFT/DSFM	Failure
I-Beam1	TZ	1544	440 truss elements for prestressing. Longitudinal reinforcing bars, stirrups, and welded mesh fabric were embedded.	Prestressing and dead load and concentrated load	DSFM	Shear
	DZ				DSFM	Shear
I-Beam2	TZ				MCFT	Shear
	DZ				DSFM	Shear
I-Beam3	TZ				MCFT	Shear
	DZ				DSFM	Shear
I-Beam4	TZ				MCFT	Shear
	DZ				DSFM	Shear
R-ElemWM		558	Prestressing bars, reinforcing bars, and welded mesh fabric were embedded	Prestressing and dead load, distributed load, and concentrated load	MCFT	Flexure*
R-Elem45					DSFM	Flexure*
R-Elem80					DSFM	Flexure
SC-BeamPC		499	45 truss elements for longitudinal reinforcing bars	Concentrated load	DSFM	Shear
SC-Beam45					DSFM	Shear
SC-Beam80					DSFM	Flexure

*Failure due to combination of longitudinal and transverse flexure.

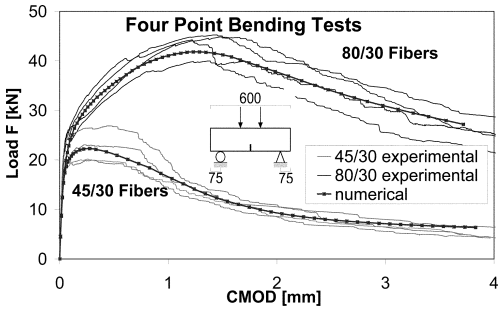

Fig. 7—Load-CMOD curves of 4PBT on beams cast with 45/30 and 80/30 fibers.

To avoid unrealistic punching failure and numerical instability problems due to load concentration, point loads and supports were simulated as nodal loads acting on a steel plate (according to the experimental procedure) having the longitudinal dimension of two finite elements and a thickness of 30 mm (Fig. 6), perfectly connected to the concrete elements.

While a single load condition was needed to analyze the Shear-Critical Beams, a two load case analysis was defined both for the I-Beam and R-Elem models as explained in the following.

Load case I

The prestrain loading was applied to the tendons and the dead load to the concrete elements. To account for the prestressing losses, a prestrain of 6.1×10^{-3} mm/mm (corresponding to a prestress of 1190 MPa) was applied to all cables instead of the original 7.2×10^{-3} mm/mm (prestress of 1400 MPa), applied during jacking. At transfer, a prestrain variable from 0 to 6.1×10^{-3} mm/mm was applied. By investigating both kinds of structures at this step, it was found that the camber calculated by the FE program was similar to the experimental one and the stress along the cable was in good agreement with most of analytical predictions. Moreover, few small cracks at the very beginning of the transfer appeared in either of the two models.

Load case II

Load case II is the application of live load. The point load (I-Beam model) or the combination of distributed and concentrated loads (R-Elem model) were increased up to failure.

MODELING OF MATERIALS

All specimens were constructed with high-performance concrete (HPC). All elements made of FRHPC were cast using 50 kg/m^3 of hooked steel fibers, whether 45/30 or 80/30 fibers.

Concrete

The three sets of specimens were cast in different times but with similar mixture designs, which led to mechanical properties of the concrete that were quite similar to each other.

Concrete mechanical properties adopted in the numerical analyses, illustrated in Table 1, are based on the results of a number of tests performed on the same mixtures used in casting the full-scale elements.

The fibers were of 30 mm in length. Two different fiber aspect ratios were adopted (aspect ratio $l/\phi = 45$ and $l/\phi = 80$); 45/30 fibers had normal strength (1250 MPa), whereas 80/30 fibers, due to higher hardening, had a higher value of ultimate strength (approximately 2300 MPa).

While all material specifications are reported elsewhere,[3,12] it is worth discussing the assumption regarding tensile behavior. Concrete in tension was assumed to be linear up to the tensile strength. The post-peak behavior, particularly important when fibers are present in the matrix, was calculated according to the Italian Standard,[14] which requires that fracture mechanics crack-mouth-opening displacement (CMOD) controlled four-point bending tests (4PBT) be performed on small beam specimens (150 x 150 x 600 mm) to determine toughness indexes and conventional residual strengths.

Figure 7 illustrates the experimental load-CMOD curves and the geometry of the 4PBTs carried out; four beams were cast with 45/30 fibers while three were with 80/30 fibers. To find a tensile stress-opening fracture constitutive relationship after the peak stress, numerical analyses were performed using a finite element program,[15] which is based on a discrete crack approach. This program considers the structure as many linear elastic subdomains, linked by interface elements that simulate cracks whose position must be known a priori. Interface elements initially connect the subdomains (as rigid links) and start activating (that is, cracks start opening) when the normal tensile stress at the interface reaches the tensile strength of the material. The crack subsequently propagates and cohesive stresses are transmitted between the crack faces according to a stress-crack opening (σ-w) law (which is given as an input for the interface elements). Figure 7 also shows the best-fitting numerical response of the 4PBT, obtained by calibrating suitable σ-w laws, indicating a close agreement with the experimental results.

The cohesive laws calculated with the finite element program had to be reduced into a cohesive stress-strain relationships (the FE routine[16] adopted implements a smeared cracking model) by dividing the fracture opening by a characteristic length value. Because well-acknowledged procedures do not exist for calculating characteristic lengths in presence of fibrous reinforcement (which is actually a matter of debate), a method was used based on the evidence of many 4PBTs carried out at the University of Brescia.[17] In fact, after the peak load, fibers generally do not show a strength higher than that offered by plain concrete. Fibers, like regular reinforcement, need a certain amount of cracking to start resisting failure. The first branch of the cohesive post-peak law of a fibrous material is thus generally similar to that of the reference material (without fibers). Therefore, it was chosen to calibrate the characteristic length of the two FRC materials, as illustrated in Fig. 8, by imposing the first post-peak branch of the σ-ε curve of plain concrete (assuming the bilinear σ-ε softening curve suggested by CEB,[18] and imposing a crack spacing of 150 mm) to be equal to the first branch of the two curves of FRC, as shown in Fig. 8 (line AB). The condition being applied led to a value of characteristic length equal to 125 mm for 45/30 fibers and 1000 mm for 80/30 fibers. Note that the higher the fracture energy G_f, the greater the characteristic length value, according to many researchers; 80/30 fibers showed a G_f four times greater than 45/30 fibers.

These relationships were then incorporated in the code of the FE routine used,[16] and were used in performing the analyses of all members containing steel fibers.

To calculate crack widths, note that the characteristic lengths were limited to the effective flexural depth of members, which represents a recognized approximate evaluation of the crack spacing of beams with little or no shear reinforcement. This especially affected the results of members with high carbon fibers (fibers 80/30), and determined different values

of characteristic lengths for the three different structural elements presented herein.

Reinforcement

The same steel types were used in all sets of structures. Based on experimental results for the tendons, a modified Ramberg-Osgood polilinear curve, suitable for low relaxation steel, was defined for the prestressing steel. Stirrups, welded wire mesh, and deformed bars were, in all cases, defined as an elasto-plastic materials with hardening by means of a multilinear stress-plastic strain curve representing the actual response of several bars tested. Table 1 also shows the yield and the ultimate stress of each type of transverse reinforcement used. Further details are provided in Reference 12.

COMPARISON OF NUMERICAL AND EXPERIMENTAL RESULTS

I-Beam specimens

As with the laboratory tests, the numerical analyses were performed with a displacement-controlled procedure, by imposing an increasing displacement at the nodes located at the middle of the steel transfer plate.

Figure 9(a) and (b) illustrate the load-displacement curves for the four I-Beam specimens in the TZ and DZ zones, respectively. Displacement was measured at the load location. Note that three identical experiments were carried out on the DZ zone of I-Beam3.

In all cases, the linear behavior is closely captured by the numerical model. The first cracking point, corresponding to the onset of nonlinearity, is adequately similar to the experimental value. Upon formation of the first tensile crack, probably owing to the smeared approach of the MCFT, the behavior in some cases is still stable and the numerical model takes slightly more load, compared to the experimental response, before showing a distinct diagonal crack.

As far as post-cracking is concerned, the FE program exhibited very good convergence in every case, although strong instability after the first cracking point was observed in the experiments. Calculated responses for the TZ zones were generally more accurate than for the DZ zones, probably due to the presence, in I-Beam2, 3, and 4, of stirrups, which produced a more stable post-peak response. Moreover, the crack pattern consisted of well distributed cracks corresponding to the well known truss model, at least up to the maximum experimental load value, as shown in Fig. 9(a) and (b). In such a situation, numerical analyses typically provide accurate simulations. In lightly or non-reinforced shear beams, however, such as I-Beam1 (both TZ and DZ model) and I-Beam2, I-Beam3, and I-Beam4 (DZ model), the behavior was governed soon after cracking by the formation of a dominant shear crack running from the load application point to the support. Here, some considerations of the local behavior, in terms of maximum crack width and local stress conditions adjacent to the crack, were examined in order to perform a proper analysis. The MCFT has been shown to provide a viable and accurate method for analysis of shear-critical beams containing little or no shear reinforcement[19] as long as two minor limits are imposed on the original constitutive relations, one relating to tensile stresses in the concrete and the other to crack widths (leading to the formulation of the DSFM). With regard to the former limit, in shear-critical unreinforced elements it has been found that using a residual concrete tensile stress of 0.1 to $0.15f_{ct}$ for concrete in tension leads to much improved

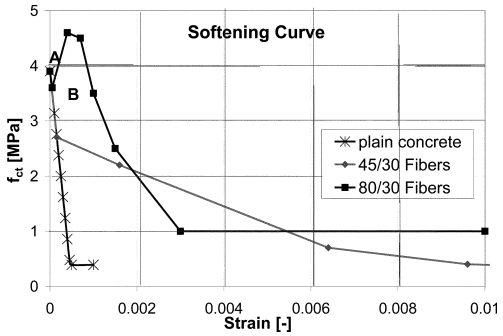

Fig. 8—Constitutive stress-strain tension softening laws adopted for fibers and plain concrete.

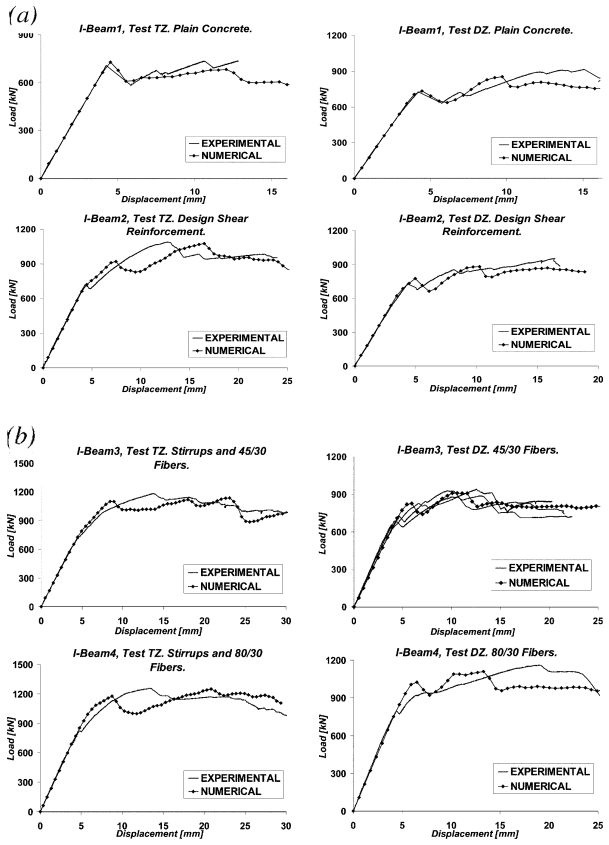

Fig. 9—Numerical and experimental load-displacement curves for: (a) I-Beam1 and I-Beam2; and (b) I-Beam3 and I-Beam4.

analytical results.[19] Concerning the crack width, shear slip along the surfaces of wide cracks can result in a divergence between the directions of principal stress and the apparent directions of principal strain. An overestimation of the reorientation of the stress trajectories and, hence, in the ductility of the beam, may result. To guard against this, the principal compressive stress was rapidly diminished in elements containing cracks exceeding a limit of 5.0 mm in width. The latter value is greater than the proposed of 2.0 mm[19] due to the huge depth and the beneficial effect of fibers, which act in reducing the instability of cracks (the measured main crack width reached values up to 20 mm in the fibrous I-Beams). That assumption resulted in a better correlation with the experimental results. In the case of I-Beam2, 3, and 4 (TZ model), which were cast with design stirrups, the crack width limit had little or no influence, as already known[19] in

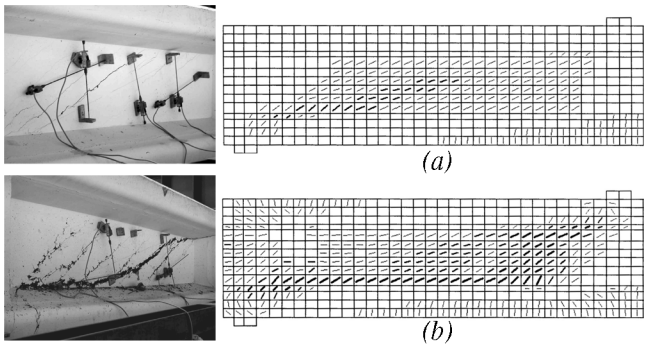

Fig. 10—Predicted and experimental crack pattern for: (a) I-Beam3, Test TZ, at first cracking; and (b) I-Beam4, Test TZ, at failure.

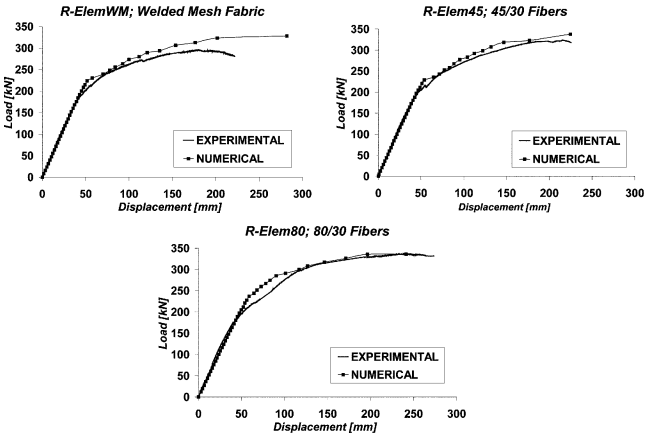

Fig. 11—Numerical and experimental load-displacement curves, R-Elem specimens.

presence of transverse reinforcement. In those beams, by inputting the experimentally measured average crack spacing of 150 mm, preferred to the program default CEB-FIB[18] code expression, the agreement with the experimental evidence increased somewhat. The average crack spacing was chosen in all other cases as a value close to the experimental one.

Moreover, it is important to note that the strong correlations achieved in the analytical modeling was in large part due to the rotating crack approach, which is a basis of the MCFT and DSFM. In fact, the experimental beams initially showed a diffused crack pattern in the panel (except in I-Beam1, made of plain concrete), which later developed through a progressive crack rotation and cracks merging together, leading to a single macrocrack oriented diagonally. This rotation led to an ultimate resisting mechanism governed by arch action and concrete residual compressive strength. The numerical model was able to capture this phenomenon, even in presence of fibers.

Fibers increased the residual compressive strength because they effectively reduced damage in tension (that is, by controlling transverse tensile strains). Examining the experimental and numerical curves for high values of vertical displacement, fibers could not offer any further residual tensile strength because the main shear crack was very wide. The load-bearing capacity, however, proved to be significantly greater in the fibrous beams than in the non-fibrous. This evidence meant that the resisting strut area, in the final arch resisting mechanism (observed especially in the DZ tests, with the main stress field running from the load point along the diagonal of the panel toward the nearest support[3,12]), must have been greater with fibers. The latter aspect is significant, particularly in terms of compression strength offered by fibers and in terms of material characterization.

The ability of the model to rotate the principal tensile strain pattern is likely a major reason for the good convergence attained in the numerical analyses, even for point-load displacements five to six times greater than the one corresponding to the first cracking point (Fig. 9(a) and (b)).

Figure 10 reports a comparison between experimental and numerical crack pattern. The first picture refers to I-Beam3, test TZ, soon after cracking, where a quite distributed crack pattern is noticeable. The second plot highlights the crack pattern at failure of I-Beam4, test TZ. One can notice the shear-dominant big crack lying below the panel diagonal. In addition, several parallel cracks, which formed at early stages according to the truss model, can still be clearly observed. In both cases, the predictions of the FE program are satisfactory and capable of describing the development of crack pattern and the corresponding changes in the resisting mechanisms. Appreciable agreement between experimental and numerical cracking can be reported in all other I-Beams.

R-Elem model

Contrary to the experiments,[20] numerical analyses were performed with a force-controlled procedure, since the specimens were stressed with both a uniform load and an eight-point concentrated load, the latter by means of a statically determinate loading system. This loading procedure turned out to be too complicated to numerically simulate. Moreover, no significant instability or global softening situation, which can not be implemented with a loading-controlled procedure, was observed.

Figure 11 depicts the external load-displacement curves at midspan for the three specimens. Note first that this diagram does not take into account the initial camber and the dead load of the structure. Moreover, the experimental displacements correspond to that at the top chord of the specimens (wings), which were affected by transverse bending after a certain point. As previously mentioned, this phenomenon was not taken into consideration since the numerical model was two-dimensional. The agreement between experiments and analytical predictions, however, is remarkably close and confirms the evidence that R-Elem80 did not exhibit any significant transverse flexure. Few transverse phenomena were instead observed in R-Elem45. The premature collapse of R-ElemWM and the overall softening response, occurring at a midspan displacement of about 200 mm, underlines the significant effect of transverse bending after that point. In this respect, the scatter between the experiment and the numerical model becomes quite important: neglecting the three-dimensional secondary effects led to numerical results that were not reliable after a midspan displacement of 200 mm; note, however, that this displacement is four times greater than the displacement at first cracking and out of any feasible design ultimate deflection.

As with the I-Beam analyses, the DSFM was applied just to the specimens without stirrups, while the simpler MCFT proved to be sufficiently reliable for R-ElemWM. The experimental crack pattern turned out to be highly diffused along the length of the member in all specimens, largely governed by longitudinal flexure and eventually combined with the transverse bending. Hence the crack width limit imposed by the DSFM proved to be less crucial in this situation. Conversely, the I-Beam model exhibited a huge

and concentrated cracking in the panel area and the pattern to failure was highly influenced by its development. Much care was therefore devoted in the I-Beam model to define the crack width, the characteristic length, and the parameters influencing the local behavior at crack.

SC-Beam model

As with the experimental tests, the numerical analyses were performed with a displacement controlled procedure.

Figure 12 illustrates the load-displacement experimental and numerical curves for the three beams, with the displacement measured at midspan.

The post-cracking behavior is overestimated somewhat by the simulations, particularly at the beginning of the non-linearity. This is probably due to the effect of tension stiffening and tension softening, which play an important role at the onset of cracking, before the complete transition to the cracked stage.

The DSFM was applied to all specimens owing to the absence of stirrups everywhere. Different crack limits were set for the specimens, in accordance with the experimental results, which showed different collapse phenomena. A sudden and very brittle shear failure was observed in SC-BeamPC, with a main shear crack 0.12 mm wide.

SC-Beam45 showed a shear failure as well, but with a much wider main shear crack and greater overall displacement, the former being 2.2 mm and the latter 26 mm. Hence, the collapse was more controlled due to the bridging effect provided by fibers, which allowed the transfer of tensile stresses along the shear-critical crack.

SC-Beam80 exhibited a flexure failure with yielding of the longitudinal deformed bars. A minor shear-critical crack formed as well, but the high carbon fibers (80/30 designation) were able to provide sufficient shear capacity and therefore alter the collapse from shear to bending, with many structural advantages consequently derived in terms of much grater ductility and higher load-bearing capacity (Fig. 12).

Figure 13 illustrates the crack pattern at the termination of the test and the corresponding crack patterns determined from the analyses. Appreciable agreement is seen between experiments and simulations: SC-Beam45 exhibited a behavior in between the two tests shown in Fig. 13; it was, in fact, possible to note fairly big cracks even in flexure, while SC-BeamPC did not exhibit any significant cracks. Specimen SC-Beam80 shows very wide cracks, especially in bending, as the experiment did (although a greater damage in shear was numerically found). Further details on shear-critical fiber-reinforced concrete beams are reported in Reference 12.

SUMMARY

The numerical modeling approach adopted, based on the MCFT and DSFM, is therefore capable of representing the linear and nonlinear behavior of the different beams tested under shear loading. It is also able to model with sufficient accuracy the fiber contribution to tension softening. Modeling fiber-reinforced concrete by inputting an appropriate tension softening behavior is a quite precise and, from a structural design point of view, a simple and effective procedure. The MCFT and DSFM formulations give excellent results in the presence of shear reinforcement; failure mode, postcracking stiffness, ultimate strength and ductility are accurately simulated. For beams containing little or no shear reinforcement or fibers, the accuracy provided by the DSFM is still quite good, although with the scatter naturally associated with mechanisms highly dependent on concrete tensile strength.

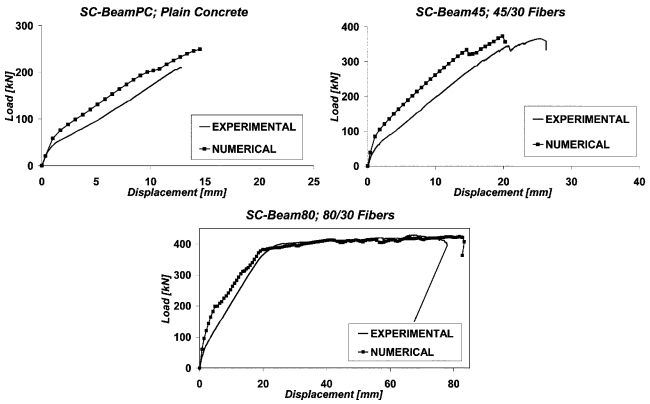

Fig. 12—Numerical and experimental load-displacement curves for SC-Beam specimens.

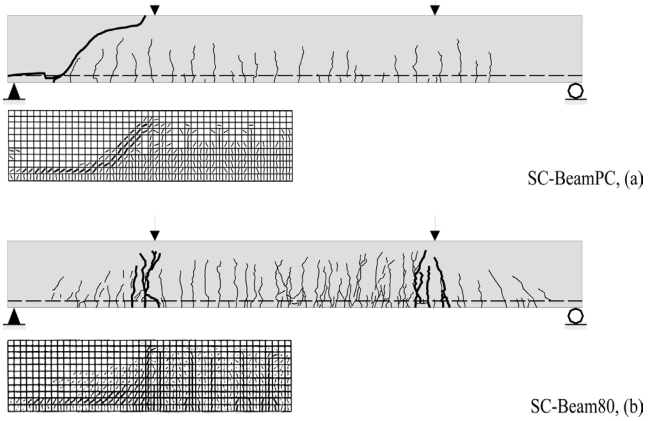

Fig. 13—Predicted and experimental crack pattern at failure for: (a) SC-BeamPC; and (b) SC-Beam80.

FURTHER RESEARCH

The corroboration studies conducted demonstrated that MCFT and DSFM can be easily adapted to fiber-reinforced concrete, provided that care is devoted to some parameters of the models, such as a proper tension softening law based on a correct characteristic length and a suitable crack width limit. Both parameters have been shown to be strongly related to the fracture energy, and even to the specimen-structure dimension. Further research should be conducted on different kinds of fiber-reinforced concretes (having basically different toughness properties under tension) in order to establish a relation between the characteristic length and the fracture energy.

Moreover, the I-Beam specimens and the SC-Beam specimens clearly demonstrated the effectiveness of fibers in increasing the residual compressive strength of FRC. The compressed strut action takes advantage of this, but there are no recognized relations or studies relating to it.

The moment-shear domain,[12,21] which defines the shear-critical beams as was shown by the SC-Model, remarkably changes due to fibers. A shear-moment domain for FRC based on suitable toughness properties would be highly useful in terms of design purposes.

Finally, in unreinforced elements, some refinement on the influence of tension stiffening effects from nearby reinforcement should be investigated.

CONCLUSIONS

In this paper, a validation of the MCFT and the DSFM, through a comparison between numerical analyses and shear

experiments on three sets of full-scale concrete and fiber-reinforced concrete beams was presented.

Numerical analyses were performed using an FE program, developed at the University of Toronto and based on the MCFT and the DSFM, suitably adapted to fiber-reinforced concrete in terms of different post-cracking behavior and local conditions at cracks. The corroboration of the model was carried out on a wide range of full-scale structures, with the test results clearly demonstrating the effectiveness of fibers in partially replacing stirrups.

The adopted model accurately predicted the post-cracking response of the members in terms of strength, stiffness, ductility, crack patterns, and failure modes. It was also able to simulate the postpeak behavior up to failure and to accurately predict the different collapse modes that occurred.

The numerical results were accurate in every case, and particularly excellent in presence of transverse reinforcing steel or when dealing with specimens that failed under bending.

The rotating crack model proved to be effective in simulating the final collapse mechanism of the I-Beam specimens, which related to arch action, involving crack reorientation and merging.

The shear contribution due to fibers and regular reinforcement was also modeled with good accuracy.

The numerical analyses, as well as the experimental results, demonstrated that shear reinforcement may be, partially or totally, effectively substituted with steel fibers, resulting in a reduction of labor cost due to the elimination of handling and placing of reinforcement.[3,12] In shear-critical beams, under certain conditions (for example, toughness and amount) fibers can postpone the shear collapse and eventually forcing a flexural failure, with a significant increase of ductility and load-bearing capacity.

These results can be used to further study the behavior of FRC beams to better understand the mechanisms governing shear failure in fiber-reinforced concrete beams and to develop a practical design procedure that accounts for the effects of fibers on beam behavior. In doing so, one must consider the two following key points:

- The fiber resistance contribution should be included with the concrete contribution,[12] whereas many researchers suggest a separate fiber shear contribution.[22] That conclusion is based on the experiments and on the numerical evidence, which demonstrates the ability of simulating FRC structures by just adopting a proper tension softening model; and
- Fibers also increase the ultimate strength of the compression strut, which is critical in some structures. The corresponding check formula, prescribed by many codes, should be adapted to FRC structures.

ACKNOWLEDGMENTS

The support of E. Giuriani and G. A. Plizzari, University of Brescia, and P. Riva, University of Bergamo, is gratefully acknowledged. The authors also wish to thank the VecTor Analysis Group at the University of Toronto for its assistance.

NOTATION

E_c = Young's modulus for concrete, measured from cylindric specimens (210 mm deep and with diameter of 75 mm)
f'_c = compressive concrete cylindric strength (28 days), assumed to be equal to $0.83f_{c,cube}$
$f_{c,cube}$ = compressive concrete strength measured from cubic specimens (150 mm edge)
f_{ct} = tensile concrete strength measured from cylindric specimens (210 mm deep and with diameter of 75 mm)
f_t = ultimate tensile strength of transverse reinforcement
f_y = yielding tensile strength of transverse reinforcement

REFERENCES

1. Meda, A., and Plizzari, G. A., "New Design Approach for Steel Fiber-Reinforced Concrete Slabs-on-Ground Based on Fracture Mechanics," *ACI Structural Journal*, V. 101, No. 3, May-June 2004, pp. 298-303.

2. Casanova, P.; Rossi, P.; and Schaller, I., "Can Steel Fibers Replace Transverse Reinforcement in Reinforced Concrete Beams?" *ACI Material Journal,* V. 94, No. 5, Sept.-Oct. 1997, pp. 341-354.

3. Meda, A.; Minelli, F.; Plizzari, G. P.; and Riva, P., "Shear Behavior of Steel Fibre Reinforced Concrete Beams," *Materials and Structures*, V. 38, Apr. 2005, pp. 343-351.

4. Noghabai, K., "Beams of Fibrous Concrete in Shear and Bending: Experiment and Model," *Journal of Structural Engineering*, V. 126, No. 2, 2000, pp. 243-251.

5. Williamson, G. R., "Steel Fibres as Web Reinforcement in Reinforced Concrete," *Proceedings*, U.S. Army Service Conference, West Point, N.Y., V. 3, 1978, pp. 363-377.

6. Di Prisco, M., and Ferrara, L., "HPFRC Prestressed Thin-Web Elements: Some Results on Shear Resistance," *IV Fracture Mechanics of Concrete Structures*, May-June 2001, V. 2, R. de Borst, J. Mazars, G. Pijaudier-Cabot, and J. G. M. van Mier, eds., A. A. Balkema Publishers, Lisse, The Netherlands, pp. 895-902.

7. Vecchio, F. J., and Collins, M. P., "Modified Compression Field Theory for Reinforced Concrete Elements Subjected to Shear," ACI JOURNAL, *Proceedings* V. 83, No. 2, Mar.-Apr. 1986, pp. 219-231.

8. Collins, M. P.; Mitchell, D.; Adebar, P.; and Vecchio, F. J., "General Shear Design Method," *ACI Structural Journal,* V. 93, No. 1, Jan.-Feb. 1996, pp. 36-45.

9. Vecchio, F. J., "Disturbed Stress Field Model for Reinforced Concrete: Formulation," *Journal of Structural Engineering*, V. 126, No. 9, 2000, pp. 1070-1077.

10. Vecchio, F. J., "Disturbed Stress Field Model for Reinforced Concrete: Implementation," *Journal of Structural Engineering*, V. 127, No. 1, 2001, pp. 12-20.

11. Vecchio, F. J.; Lai, D.; Shim, W.; and Ng, J., "Disturbed Stress Field Model for Reinforced Concrete: Validation," *Journal of Structural Engineering*, V. 127, No. 4, 2001, pp. 350-358.

12. Minelli, F., "Plain and Fiber Reinforced Concrete Beams under Shear Loading: Structural Behavior and Design Aspects," PhD thesis, University of Brescia, Brescia, Italy, Feb. 2005, 422 pp.

13. EUROCODE 2 1993, "Design of Concrete Structures," UNI-ENV 1992-1-2.

14. UNI 11039, "Steel Fiber Reinforced Concrete—Part I: Definitions, Classification Specification and Conformity—Part II: Test Method for Measuring First Crack Strength and Ductility Indexes," Italian Board for Standardization, 2003.

15. Reich, R.; Cervenka, J.; and Saouma, V. E., "MERLIN, a Three-Dimensional Finite Element Program Based on a Mixed-Iterative Solution Strategy for Problems in Elasticity, Plasticity, and Linear and Nonlinear Fracture Mechanics," *EPRI,* Palo Alto, Calf., 1994.

16. Wong, P. S., and Vecchio, F. J., "VecTor2 and FormWorks User's Manual," *Technical Report*, Department of Engineering, University of Toronto, Toronto, Ontario, Canada, Aug. 2002, 217 pp. (available at http://www.civ.utoronto.ca/vector/).

17. Cangiano, S.; Cucitore, R.; and Plizzari G. A., "A New Proposal for the Evaluation of Fracture Properties of Steel Fiber Reinforced Concrete," *6th International Symposium on Utilization of High Strength/High Performance Concrete*, G. König, F. Dehn, and T. Faust, eds., Lipsia, Germany, June 16-20, 2002, V. 2, pp. 873-886.

18. CEB-FIP, "Model Code for Concrete Structures: CEB-FIP International Recommendations," 3rd Edition, Comité Euro-International du Béton, Paris, 1978, pp. 348.

19. Vecchio, F. J., "Analysis of Shear-Critical Reinforced Concrete Beams," *ACI Structural Journal,* V. 97, No. 1, Jan.-Feb. 2000, pp. 102-110.

20. Minelli, F.; Cominoli, L.; Meda, A.; Plizzari, G. A.; and Riva, P., "Full Scale Tests on HPSFRC Prestressed Roof Elements Subjected to Longitudinal Flexure," *International Workshop on High Performance Fiber Reinforced Cementitious Composites in Structural Applications*, Honolulu, Hawaii, May 23-26, 2005 (available at http://www.hpfrcc-workshop.org/).

21. Imam, M.; Vandewalle, L.; Mortelmans, F.; and Van Gemert, D., "Shear Domain of Fibre-Reinforced High-Strength Concrete Beams," *Elsevier Engineering Structures*, V. 19, No. 9, 1997, pp. 738-747.

22. RILEM Final Recommendations TC-162-TDF, "Test and Design Methods for Steel Fibre Reinforced Concrete; s-e Design Method," *Materials and Structures*, V. 36, Oct. 2003, pp. 560-567.